

1 **Measurement report:**

2 **Intra-annual Variability of Black/Brown Carbon and Its Interrelation with**
3 **Meteorological Conditions over Gangtok, Sikkim**

4 Pramod Kumar¹, Khushboo Sharma¹, Ankita Malu², Rajeev Rajak², Aparna Gupta¹,
5 Bidyutjyoti Baruah¹, Shailesh Yadav¹, Thupstan Angchuk¹, Jayant Sharma¹, Rakesh Kumar
6 Ranjan^{1#}, Anil Kumar Misra¹, and Nishchal Wanjari¹

7 ¹DST's Centre of excellence on Water Resources, Cryosphere and Climate Change Studies,
8 Department of Geology, Sikkim University, Gangtok, Sikkim, India -737102

9 ²Department of Geology, Sikkim University, Gangtok, Sikkim, India -737102

10 #Corresponding Author: rkranjan@cus.ac.in

11
12 **Abstract**

13 Black carbon (BC) and brown carbon (BrC) have versatile natures, and they have an apparent
14 role in climate variability and changes. As the anthropogenic activity is surging, the BC and
15 BrC are also reportedly increasing. So, the monitoring of BC/BrC and observation of land use
16 land cover changes (LULCC) at a regional level are necessary for the various interconnected
17 meteorological phenomena changes. The current study investigates BC, BrC, CO₂, BC from
18 fossil fuels (BC_{ff}), BC from biomass burning (BC_{bb}), LULCC, and their relationship to the
19 corresponding meteorological conditions over Gangtok in the Sikkim Himalayan region. The
20 concentration of BC (BrC) 43.5 µg/m³ (32.0 µg/m³) was found to be highest during the March-
21 2022 (April-2021). Surface pressure exhibits a significant positive correlation with BC, BC_{ff},
22 BC_{bb}, and BrC. Higher surface pressure results in a calmer and more stable boundary layer,
23 which effectively retains accumulated contaminants. Conversely, the wind appears to facilitate
24 the dispersion of pollutants, showing a strong negative correlation. The fact that all pollutants
25 and precipitation have been shown to behave similarly points to moist scavenging of the
26 pollutants. Despite the dense cloud cover, it is clear that the area is not receiving convective
27 precipitation, implying that orographic precipitation is occurring over the region. Most of
28 Sikkim receives convective rain from May to September, indicating that the region has
29 significant convective activity contributed from the Bay of Bengal during the monsoon season.
30 Furthermore, monsoon months have the lowest concentrations of BC, BC_{bb}, BC_{ff}, and BrC,
31 suggesting the potential of convective rain (as rain out scavenging) to remove most of the
32 pollutants. Moreover, BC and BrC show positive radiative feedback.

33 **Keywords:** Black carbon; Brown carbon; LULC; Sikkim Himalaya; Meteorology; Biomass
34 burning; Radiative forcing.

35 **1.0 Introduction**

36 Black carbon (BC), and brown carbon (BrC), are part of fine particulates in air pollution that
37 have a deceptive role in climate variability and changes. BC/BrC is a short-lived climate
38 pollutant with a lifetime of only days to weeks after release in the atmosphere (Pierrehumbert,
39 2014). During this short period of time, BC/BrC can have significant direct and indirect
40 impacts on the climate, cryosphere, agriculture, and human health (Shindell et al., 2012). It
41 consists of pure carbon in several interconnected forms. BC is formed through the incomplete
42 combustion of fossil fuels, biofuel, and biomass, and is one of the main types of particles in
43 both anthropogenic and naturally occurring soot (Bond et al., 2004). BrC in the atmosphere
44 has been attributed to the burning of biomass and fossil fuels, the biogenic release of fungi,
45 plant debris, and humic matter, and multiphase reactions between the gas-phase, particulate,
46 and cloud microdroplet constituents in the atmosphere (Laskin et al., 2015). BC/BrC is
47 transported from its source to many locations across the world (Ramanathan and Carmichael,
48 2008). The BC/BrC released into the atmosphere exhibits vertical distribution and follows the
49 prevailing wind speed and direction. It engages with various atmospheric components before
50 eventually settling on the Earth's surface through either wet or dry deposition processes. Its
51 hygroscopic properties render it more prone to cloud seeding and cloud formation, thereby
52 contributing directly to the precipitation mechanism in regions with high humidity (Stevens
53 and Feingold, 2009). In addition, it absorbs both incoming and outgoing radiation, atmospheric
54 BC/BrC modifies radiative forcing, disturbs atmospheric stability, regional circulation, and
55 rainfall pattern, affects cloud albedo, material damage, reduces agricultural productivity,
56 degrades ecosystem, and affects human health (Zhang et al., 2013). However, due to an
57 insufficiency of observations, BrC is one of the least understood and uncertain warming agents
58 (Yue et al., 2022). Numerous studies have been conducted to analyze the global distribution
59 of BC and BrC, including research focused on these species within India as well (Reddy and
60 Venkataraman, 2002a, 2002b; Venkataraman et al., 2006; Park et al., 2010; Sloss, 2012; Helin
61 et al., 2021; 2020; Kumar et al., 2020a; Watham et al., 2021; Bhat et al., 2022; Runa et al.,
62 2022; Yue et al., 2022; Kumar et al, 2018b). However, the overall worldwide BC emission is
63 estimated to be 4800-7200 Gg per year (Klimont et al., 2017). In 2001, India's total BC
64 emissions were projected to be 1343.78 Gg (Sloss, 2012). Residential fuel burning and
65 transportation contribute maximum to the global anthropogenic BC emission (Helin et al.,
66 2021). About 60 to 80% of residential fuels (coal and biomass) emissions are reported from
67 Asian and African countries, whereas approximately 70% of diesel engine emissions are found

68 to be from Europe, North America, and Latin America (Johnson et al., 2019; Ayompe et al.,
69 2021; Adeeyo et al., 2022; Sun et al., 2022).

70 On the other hand, emissions on the Indian subcontinent have increased by 40% since the year
71 2000 (Kurokawa and Ohara, 2020; Sun et al., 2022). According to Reddy and Venkataraman
72 (2002a, 2002b), the estimated BC emissions in India are fossil fuels, 100 Gg biofuel, 207 Gg
73 open burning, and 39 Gg with a climatic forcing of $+1.1 \text{ W/m}^2$, black carbon is the second-
74 most significant human emission in the current atmosphere (Sharma et al., 2022). BC
75 concentration was measured by Zhao et al. (2017) in the south-eastern Tibetan Plateau (TP).
76 Daily mean BC loadings ranged from 57.7 to 5368.9 ng/m^3 demonstrating a high BC burden
77 even at free tropospheric altitudes (Zhao et al., 2017). Black carbon (BC) deposition was
78 estimated at the Nepal Climate Observatory - Pyramid (NCO-P) site in the Himalayan region
79 during the pre-monsoon season (March-May). A total BC deposition rate of $2.89 \mu\text{g/m}^3/\text{day}$
80 was estimated, resulting in a total deposition of $266 \mu\text{g/m}^3$ for March–May (Yasunari et al.,
81 2010). From the Indian perspective, several key short-term incidents contribute to a rise in
82 India's BC concentration from biomass burning and other sources (Kumar et al., 2020a).
83 Burning agricultural waste (stubble) is widespread in India and several other nations. Many
84 studies suggest that increased BC in northern India, notably the Indo-Gangetic Plain (IGP) is
85 the global absorbing aerosol hotspot (Venkataraman et al., 2006; Ramanathan and Carmichael,
86 2008). In India, post-monsoon paddy crop waste burning occurs in the months of October and
87 November in the north and northwest parts of India (Venkataraman et al., 2006). In the north-
88 western Indo-Gangetic Plain (IGP) (especially- Punjab, Haryana, and western Uttar Pradesh),
89 stubble burning is a popular practice (Venkataraman et al., 2006). Long-distance transport of
90 BC aerosols, mostly from Asia to the North Pacific and South America to the southwest
91 Atlantic, is often recognized as a significant factor in local concentration (Evangelista et al.,
92 2007). However, in India, only local sources (89%) affect BC concentrations (Zhang et al.,
93 2013), as there aren't many movements of transboundary aerosols contribution over the IGP
94 (Kumar et al., 2018a; Kedia et al., 2014; Ramachandran and Rupakheti, 2022; Ramachandran
95 et al., 2020). Both marine and continental air masses contributed to total aerosol loading over
96 middle-IGP (Kumar et al., 2017; Shukla et al., 2022).

97 Black carbon is a light-absorbing particle that is released into the atmosphere directly in the
98 form of ultrafine ($<0.1 \mu\text{m}$) to fine particles ($<2.5 \mu\text{m}$) (Gupta et al., 2017). BC is a good tracer
99 for particle deposition as it is non-volatile, insoluble, and chemically inert, and it can also mix
100 well with other aerosol species in the atmosphere (Kiran et al., 2018). As a result, BC
101 deposition data are important not just for BC sinks but also for a broader understanding of

102 aerosol deposition. BC emissions are mostly influenced by significant changes in the energy
103 sector, fuel usage, industrial expansion, and an increase in the number of vehicles (Bisht et al.,
104 2015). Residential fuels like wood, agricultural waste, and cow dung used for cooking and
105 biomass usage for home purposes are the primary sources of BC emissions (Venkataraman et
106 al., 2006). The Asian mainland is a substantial contributor to global BC emissions and has
107 been identified as a hotspot (Gupta et al., 2017). BC has a high absorption ability, accounting
108 for 90-95 percent of total atmospheric aerosol absorption (Hansen et al., 1984). It can absorb
109 solar energy in the visible-infrared band and warm the environment. In comparison to carbon
110 dioxide, BC has a much shorter life cycle in the atmosphere. As a result, mitigation or reduction
111 has a greater positive impact on the atmosphere (Kirchstetter et al., 2004; Takemura and
112 Suzuki, 2019). Changing land use land cover (LULC) has a very significant impact on weather,
113 climate, and aerosols (Mahmood et al., 2010). It is well well-stabilised fact that the LULC
114 change has a direct relation with land surface temperature, vehicular emission, and
115 anthropogenic activity (Aithal and MC, 2019). This motivated the present study for further
116 analysis of Sikkim region land use land cover change and its relation with temperature and
117 BC/BrC for March 2021 to March 2022. The current study's objectives are to assess the intra-
118 annual variability of Black/Brown Carbon (BC/BrC) (diurnal/daily/monthly) during the study
119 period March-2021 to March-2022, as well as the interrelationship between meteorological
120 conditions and BC/BrC, along with LULC change for three decades 2000, 2010, and 2020, and
121 its relationship with anthropogenic activity over Gangtok.

122 **2.0 Study location**

123 The Gangtok Municipal Corporation (GMC) has been selected for the present study on the
124 basis of its urban exposure and settlement change for three decades as well as congruently
125 temperature rise (Figure S1). The sampling was carried out at the Pani House area in Gangtok,
126 GMC, having a longitude of 88.609°E and a latitude of 27.323°N. Sikkim is surrounded by
127 Nepal, China, and Bhutan from west, north, and east respectively, and consists of the trans and
128 greater Himalayan range. Moreover, Sikkim has one of the most fragile forest covers.
129 However, Gangtok is a densely populated city and capital of the state of Sikkim which is
130 situated in the East Sikkim district (see Figure 1a). The population of Sikkim has been found
131 to have increased as per the Indian census for three decades as can be seen in table S1.

132 **3.0 Data and Methodology**

133 The real-time sampling of BC was carried out from 10th March 2021 to 17th March 2022, at
134 Gangtok using the seven-channel dual spot Aethalometer (Model AE-33-7, Magee Scientific,

135 USA). The data was collected for the measurement of BC and BrC associated with particulate
136 matter having an aerodynamic diameter of less than 2.5 μm ($\text{PM}_{2.5}$). The concentration of BC,
137 BrC, BC_{bb} , and BC_{ff} have been estimated by the Carbonaceous Aerosol Analysis Tools
138 (CAAT) software tool from the Magee Scientific Aethalometer model AE33 (Hansen and
139 Schnell, 2005). The carbon dioxide (CO_2) was measured using a CO_2 sensor (Vaisala-
140 GMP343) which is attached to the aethalometer. The inlet of the aethalometer was mounted at
141 a height of 15 m above ground level. One of the main sources of uncertainty in using aerosol
142 absorption measurements to estimate the BrC absorption coefficient at 370 nm is the fact that
143 other species, such as black carbon and dust, can also contribute to the measured absorption.
144 This can lead to overestimation of BrC mass concentration, particularly in environments where
145 these species are also present. However, the Sikkim region has one of the highest precipitation
146 regions in the world and negligible contribution to dust pollution. Furthermore, there must be
147 lesser over/underestimation. Therefore, the present study used mass concentration.

148 A new data set of BC, BrC, Black Carbon from biomass burning (BC_{bb}), Black Carbon from
149 fossil fuels (BC_{ff}), the percentage contribution of biomass burning to BC (BB%) and CO_2 has
150 been generated over the unreported region of Sikkim Himalaya. The diurnal and monthly data
151 sets of BC, BC_{bb} , BC_{ff} , BrC, BB%, and CO_2 have been given in the details in supplementary
152 materials (Table S2 and S3). In addition to this, the meteorological data has been selected for
153 ERA5 reanalysis for the study. LULC data has been taken from USGS earth explorers of 2000
154 and 2010 Landsat-5, 2020 Landsat-8, and 2021 for Sentinel-2 (Karra et al., 2021). LULC data
155 has been chosen for the month of December to minimize the cloud cover. The details of the
156 LULC calculation steps used are given in the supplementary section (methodology S1.3). The
157 brief of the data set is discussed in the table 1.

158 **3.1 Estimation of BrC**

159 The Carbonaceous Aerosol Analysis Tools (CAAT) software tool from the Magee Scientific
160 Aethalometer model AE33 was utilized to estimate the concentrations of BC, BrC, BC_{bb} , and
161 BC_{ff} . The absorption coefficients of BC and BrC were determined using the multi-wavelength
162 absorption coefficients provided by the aethalometer. The presence of BrC was identified by
163 observing the maximum light absorption between 370–590 nm, but its absorption may increase
164 significantly below this range depending on its composition. The attenuation of illumination
165 measured in this study using the aethalometer was attributed solely to the contribution of BC
166 and BrC. It is believed that the absorption coefficient at 370 nm measured by the aethalometer
167 represents the combined absorption coefficients of BC and BrC, which is denoted as $\sigma_{\text{BC} + \text{BrC}}$

168 (370 nm). This assumption is similar to the model used in the multi-wavelength absorbance
 169 analyzer (MWAA) approach for source allocation, as described in Massabò et al. (2015).
 170 Equation (1) was used to calculate the σ_{BrC} (370 nm) absorption coefficient (supplementary
 171 methodology S1), which involved subtracting the contribution of BC (σ_{BC} (370 nm)) from the
 172 observed absorption coefficient (σ_{BC+BrC} (370 nm)).

$$173 \quad \sigma_{BrC}(370 \text{ nm}) = \sigma_{BC+BrC}(370 \text{ nm}) - \sigma_{BC}(370 \text{ nm}) \quad \text{Eq. (1)}$$

174 The σ_{BC} (370 nm), was calculated by applying the power-law fit to absorption data in the 590-
 175 950 nm wavelength range provided in equation (1).

$$176 \quad \sigma_{BC}(\lambda) = \beta \lambda^{-AAE_{BC}} \quad \text{Eq. (2)}$$

177 The absorption angstrom exponent of BC is denoted as AAE_{BC} , with β being a constant value.
 178 As BC is a significant contributor to light absorption at wavelengths beyond 590 nm, the
 179 contribution of other aerosol species can be neglected, and the AAE_{BC} can be calculated using
 180 equation (3), as stated in Rathod and Sahu (2022). The AAE for both BC and BrC can be
 181 expressed as σ , and in this study, the AAE definition by Moosmüller et al. (2011a) was used
 182 instead of the AAE specified for a wavelength pair. This value is determined by equation (3),
 183 which calculates the negative log-log slope of the absorption spectrum at wavelength λ .

$$184 \quad AAE_{BC} = -\frac{d \ln \sigma_{BC}}{d \ln \lambda} \quad \text{Eq. (3)}$$

185 Instead of the conventional approach where AAE_{BC} is assumed to be 1, we utilized the AAE_{BC}
 186 that was observed onsite to calculate $\sigma_{BC}(\lambda)$. Equation (4) was employed to determine σ_{BrC}
 187 (370 nm) by substituting $\sigma_{BC}(\lambda)$ at 370 nm, which was obtained using equation (2) (Wang et
 188 al., 2020), into equation (4) (refer to supplementary methodology S1.1, S1.2, and Figure S2
 189 for details).

$$190 \quad \sigma_{BrC}(370 \text{ nm}) = \sigma_{BC+BrC}(370 \text{ nm}) - \beta(370 \text{ nm})^{-AAE_{BC}} \quad \text{Eq. (4)}$$

191 To calculate $\sigma_{BrC}(\lambda)$ at 470 nm and 520 nm, we can subtract the modelled BC from the
 192 measured absorption coefficients, in a similar manner. It is worth noting that the BrC
 193 absorption coefficients are very low at wavelengths beyond 590 nm (Wang et al., 2020),
 194 according to Rathod et al. (2017) and Rathod and Sahu (2022), hence they are not taken into
 195 account (supplementary methodology S1).

196 **3.2 Data Analysis**

197 LULC change also has a direct impact on vehicular emissions and other anthropogenic
 198 activities. Urbanization, conceivably, can lead to increased vehicle traffic and emissions,
 199 which can contribute to air pollution and climate change. Changes in land use can also affect
 200 the amount and type of vegetation, which can influence the carbon cycle and the amount of
 201 greenhouse gases in the atmosphere. The ERA-5 reanalysis data has been used for
 202 meteorological analysis viz. wind pattern, precipitation, relative humidity, and temperature
 203 (Hersbach et al., 2020). The hourly data has been taken for the analysis and then the daily,
 204 monthly, and seasonal average has been computed for the study period over the Sikkim and
 205 surrounding states for a better understanding of the meteorological conditions influencing the
 206 BC, and BrC. The ERA5 validation with AWS data can be seen in the supplementary section
 207 (Figure S8). The total precipitation is computed as a sum of the hourly data for a day to daily
 208 total precipitation and further, it was summed for monthly cumulative total precipitation using
 209 the sum formula as

$$210 \quad \text{Monthly Cumulative Total Precipitation} = \sum_i^n X \quad \text{Eq. (5)}$$

211 Where ‘i’ is the initial ‘n’ the last date and X is the hourly total precipitation taken from ERA5.
 212 The wind circulation has been computed using the u-component and v-component of wind and
 213 the wind speed has been calculated as

$$214 \quad \text{Wind Speed} = \sqrt{u^2 + v^2} \quad \text{Eq. (6)}$$

215 The temperature and relative humidity averaged have been computed using the mean formula
 216 as

$$217 \quad \text{Average} = \frac{\sum_i^n X}{n} \quad \text{Eq. (7)}$$

218 Where, ‘i’ is the initial and ‘n’ last date of the variables such as temperature, relative
 219 humidity, and wind components.

220 Let x and y be two real-valued random variables such that the correlation coefficient Spearman
 221 Pearson can be calculated between the BC/BrC and meteorological parameters. The
 222 Coefficient of Pearson Correlation (PCC) (Pearson, 1909; Benesty et al., 2009) as

$$223 \quad PCC = \frac{n(\sum xy) - (\sum x)(\sum y)}{\sqrt{[n \sum x^2 - (\sum x)^2][n \sum y^2 - (\sum y)^2]}} \quad \text{Eq. (8)}$$

224 Where ‘n’ is the population size of the variables used for the study.

225 Table 1 contains additional information about the dataset, and a more detailed methodology
226 can be found in the supplementary section (S1).

227 **4.0 Results and Discussions**

228 The anthropogenic activities in Gangtok have drastically increased in the last 20 years. As
229 evident from Figures 1b, c, and d, LULC has been changed from 2000 to 2020 over the
230 Gangtok Municipal Corporation (GMC). Population change and growth have also been
231 observed in the Sikkim (Table S1). LULC during the years 2000 and 2010 evidently shows
232 that most of the fallow land has been built up due to a recent change in the policy of
233 construction in Sikkim suggesting urban settlement load over Gangtok has increased
234 significantly. As a result, there is a significant increase in built-up areas in GMC for the last
235 20 years. The vegetation cover has also reduced from 2000 to 2020 (Figure 1b, c, and d). The
236 rainfed water bodies are reducing from the GMC. However, due to its seasonal nature, streams
237 are lesser emerged in 2020. Which perhaps shows the precipitation pattern alteration over
238 GMC due to the highly built-up sprawl. The built-up extent has been sprawling and consuming
239 the dense vegetation regions as well. This increases the study region's urge to be acknowledged
240 so that Sikkim's future policymakers can consider the effects of rising anthropogenic activities.
241 This anthropogenic activity leads to a heavy load on the environment over one of the cleanest
242 states of India. Long-term spatiotemporal variation of 2-meter air temperature justifies the
243 LULC change and warming pattern (Xiao-lei et al., 2022) over the Gangtok region (Figure
244 S1a, S1b, S1c, S1d, and S1e). The decadal warming rate is varying from 0.25° to 0.45°C
245 (Figure S1e). Thereafter, BC and BrC over the Gangtok have been measured to report the issue
246 and get more attention to the scientific and local community. The higher anthropogenic activity
247 releases a higher amount of emission in the name of development due to the population load
248 on the region (Shaddick et al., 2020) (i.e., the growth rate has been raised from 12.89 to 13.05%
249 in recent years) (Table S1). Diurnal variation of the BC, BrC, BC_{bb}, BC_{ff}, and CO₂ show two
250 peaks. BC, BC_{ff}, and CO₂ have almost similar time of peaks observed. The first peak is found
251 during 8-10 AM. And, the second peak is observed during 8-10 PM. However, BrC and BC_{bb}
252 have the peak concentration during 10-11 AM and 6-8 PM (Figure 2a), suggesting the peak
253 biomass burning time over the region. The meteorological conditions are observed as low
254 dewpoint, low temperature, high surface pressure, low wind speed, and high relative humidity
255 to the corresponding 8-10 AM, while the opposite is found in 8-10 PM referred to Figure 2b.

256 The daily time series of the BC, BC_{bb}, BC_{ff}, BrC, BB%, and CO₂ show the highest fluctuation
257 from 20th to 30th March in both 2021 and 2022 years respectively. The maximum BC (BrC)

258 content was found in March 2022 (April-2021), at $43.5\mu\text{g}/\text{m}^3$ ($32\mu\text{g}/\text{m}^3$). The lowest
259 fluctuation is observed from 15th May to 15th September 2021 (Figure 3a). The intense peaks
260 of BC, BC_{ff}, and CO₂ were observed from 10th October to 15th November 2021 (Figure 3a)
261 which may be linked to the heavy tourist season of the state and indicate the traffic overload
262 in the Gangtok (Sharma et al, 2022). The meteorological conditions also favour similar
263 circumstances to accumulate the pollutant from 10th October to 15th November 2021 (Figure
264 3b). The lowest surface pressure with minimum fluctuation and the highest temperature and
265 dewpoint temperature with minimum fluctuation was noticed from the 15th June to 20th
266 September 2021 (Figure 3b). BrC is found to be the highest with significant variability from
267 the 10th of January to the 30th of March, pointing to winter wood burning for livelihood, which
268 is also supported by BC_{bb} (Table S3). The monthly variations of BC, BC_{bb}, BC_{ff}, BrC, and
269 BB% are discussed in Figure 4a, and the highest value of standard deviation was observed
270 during March 2022 for BC, BC_{ff}, and April 2021 for BC_{bb}, BrC, and BB%. The CO₂ is
271 observed almost constant with a small value of standard deviation. The maximum
272 concentration of the BC, BC_{ff} is found in March 2022. However, BC_{bb} and BrC were measured
273 highest in April 2021 (Table S3). This is probably inferring to high tourist season (i.e.,
274 vehicular emission) as well as random wood burning at higher altitude regions surrounding the
275 Gangtok. The minimum concentration of the BrC was seen in the month of August 2021 as the
276 highest total precipitation month with high wind speed, temperature dewpoint temperature,
277 and relative humidity (Figure 4b, S3, and S4) (Rana et al., 2023).

278 The good correlation between BC and BC_{ff} showed that the primary source of BC is fossil fuel
279 combustion (Osborne et al, 2008; Jung et al., 2021). A significant correlation between BC_{bb}
280 and BrC indicates that biomass burning is a major contributor to BrC (Prabhu et al., 2020),
281 which is supported by the BB% and BrC (Figure 5). The positive correlation between CO₂ and
282 BC/BC_{ff} suggests that fossil fuel burning is influencing the CO₂ concentration (Rana et al.,
283 2023). Dewpoint temperature and CO₂ have a significant positive correlation suggesting
284 positive radiative forcing of the CO₂ (Huang et al., 2017; Stjern et al., 2023). A similar has
285 been found for the temperature. BC_{bb}/BrC and temperature have a strong significant negative
286 correlation suggesting the negative radiative nature of the BC_{bb}/BrC (Figure S5). Moreover,
287 net thermal/solar radiation (STR/SSR) and BC/BrC have a significant positive correlation
288 (Figure 5, and S5) (Liu et al., 2020). A strong significant positive correlation between surface
289 pressure and BC/BC_{ff} (BC_{bb}/BrC) has been observed (Figure 5). Higher surface pressure
290 creates calm conditions and a stable boundary layer, which keeps the pollutants accumulated
291 in the boundary layer (Igarashi et al., 1988; Lee et al., 1995; Bharali et al., 2019; Liu et al.,

292 2021). However, the opposite has been observed for the wind indicating the dispersion of
293 pollutants with a strong negative correlation. A similar has been observed for the total
294 precipitation and all the pollutants, delineating to wet scavenging of the pollutants (Yoo et al.,
295 2014; Ohata et al., 2016; Ge et al., 2021; Wu et al., 2022). The relative humidity is also showing
296 a similar result to the total precipitation with greater values of coefficient. The negative
297 correlation between total precipitation and surface pressure suggests that the rain falls over the
298 region mostly occurs in a low-pressure system that is caused due to the vertical rising of an air
299 parcel and causes condensation and precipitation (Johnson and Hamilton, 1988; Sarkar, 2018).
300 However, cloud condensation nuclei formation and precipitation are prompted by aerosols (BC
301 and BrC) (Ohata et al., 2016; Moteki, 2023). Moreover, BC particles are mainly hydrophobic
302 and less efficient as CCN compared to more hydrophilic particles; they can still act as CCN
303 under certain conditions. These conditions include the size and mixing state of the particles, as
304 well as the atmospheric conditions such as relative humidity and temperature (Ohata et al.,
305 2016; Moteki, 2023; Liu et al., 2020). The conditions required for BC particles to efficiently
306 play the role of CCN depend on several factors, including their size, mixing state, and
307 atmospheric conditions (Moteki, 2023; Liu et al., 2020). For example, smaller BC particles are
308 more efficient as CCN than larger ones (Moteki, 2023). The mixing state of BC particles also
309 plays a role, as externally mixed BC particles are less efficient as CCN than internally mixed
310 ones (Liu et al., 2020). Atmospheric conditions such as relative humidity and temperature also
311 affect the efficiency of BC particles as CCN (Moteki, 2023). For example, higher relative
312 humidity and lower temperatures can increase the efficiency of BC particles as CCN (Moteki,
313 2023). Additionally, relative humidity over the study region is very high during the entire year
314 with the favorable temperature. Thereafter, BC and BrC have a crucial role in the precipitation
315 mechanism (Zhu et al., 2021; Li et al., 2023a) over the study region. Total precipitation and
316 wind circulation indicated that the study region received precipitation throughout each month
317 of the study period (i.e., most of the time in the form of rain and occasionally snow). Hence
318 the maximum is observed in August and the minimum in March 2022. The wind pattern
319 illustrates the monsoon seasonal strong influence from May to September 2021 (Figure 6). The
320 wind converges in the valley and diverges from the mountain for the rest of the period (figure
321 6). Because the strong wind and heavy rainfall indicated pollution scavenging (rain out or wash
322 out), it is significantly negatively correlated as TP vs BC_{bb}; TP vs BC_{ff}; TP vs BrC (Figure 5).
323 The relative humidity and temperature follow the same pattern when the temperature gradients
324 change from January to December, resulting in a decrease in moisture content in the
325 atmosphere (Figure S6). The lowest in the month of February is observed and the temperature

326 gradient gets steep from November (Figure S6). The dewpoint temperature contour and surface
327 pressure shading match well suggesting that the surface pressure creates the dewpoint
328 temperature gradient and keeps it sustained and stable atmospheric condition (Jung et al., 2023)
329 (Figure S7). During the month of June, it is very peculiar that the dewpoint temperature
330 contours are wide and a very small gradient is observed (Figure 7). This points toward the
331 warm conditions during the June over entire Sikkim. The cloud cover and convective
332 precipitation over Sikkim are discussed in Figure 7. It is clear from (Figures 7a to d) that the
333 region is not receiving much convective precipitation even if there is huge cloud cover, which
334 leads to a conclusion of orographic precipitation over the region (Figure 7). However, the
335 relative humidity is very high over the sampling site from the lower to upper middle level of
336 the atmosphere during the study period (Figure S3). Most of Sikkim receives convective rain
337 from May to September, which indicates that the region has strong convective activity added
338 from the Bay of Bengal during the monsoon season (Rahman et al., 2012; Kumar et al., 2020b;
339 Kakkar et al., 2022; Biswas and Bhattacharya, 2023). Again, from October to April, the region
340 does not receive convective rain even though there is strong cloud cover pointing toward the
341 orographic rainfall over the entire Sikkim (Kumar and Sharma, 2023). That's making the
342 Sikkim unique weather conditions (Figures S3 and S4). The ERA5 validation with AWS data
343 can be seen in the supplementary section (Figure S8). And, the least concentration of BC, BC_{ff},
344 BC_{bb}, and BrC is observed during the monsoon months. This observation supports the
345 convective rain, as rain out scavenging, of all pollutants (Liu et al., 2020; Moteki, 2023).
346 During the monsoon season, the region experiences high convective activity, which is added
347 from the Bay of Bengal (Brooks et al., 2019; Liu et al., 2020; Moteki, 2023; Sankar et al.,
348 2023). Convective rain is an effective process for removing air pollutants from the atmosphere
349 (Liu et al., 2020; Moteki, 2023). Wet removal of BC and BrC occurs via cloud particle
350 formation and subsequent conversion to precipitation or impaction processes with
351 hydrometeors below clouds during precipitation (Liu et al., 2020; Moteki, 2023; Sankar et al.,
352 2023). The BC and BrC have a significant positive correlation with thermal and solar radiation,
353 indicating positive radiative feedback (Zhang et al., 2020; Wang et al., 2021; Li et al., 2023a).
354 A stronger negative correlation between CO₂ and surface thermal radiation (STR) and surface
355 solar radiation (SSR) would have significant implications (Figure 5). The negative correlation
356 between CO₂ and STR implies that as the concentration of CO₂ in the atmosphere increases,
357 the amount of heat radiating from the Earth's surface into space decreases (Zhang et al., 2020).
358 This can lead to an increase in the Gangtok's temperature, which can have various impacts on
359 climate and weather as well (Figures S1, and 5). The negative correlation between CO₂ and

360 SSR implies that as the concentration of CO₂ in the atmosphere increases, the amount of solar
361 radiation absorbed by the Earth's surface decreases (Davis, 2017; Zhang et al., 2020; Li et al.,
362 2023b) (Figure 5). Overall, a significant negative correlation between CO₂ and STR/SSR
363 would indicate a stronger influence of greenhouse gas concentrations on the surface's radiation
364 balance (Chiodo et al., 2018) and would have important implications for climate change as
365 well as anomalous warming over the Gangtok region (Figure S1).

366 **5.0 Conclusions**

367 In accordance with the LULC between 2000 and 2010, Sikkim's recent changes to its
368 development regulations have resulted in the majority of fallow land being consumed by
369 construction, which suggests that Gangtok's urban settlement load has increased significantly.
370 In addition, the LULC for 2020 depicts a booming built-up region over the GMC. From 2000
371 to 2020, the vegetation cover has likewise decreased. However, due to the seasonal nature,
372 streams are lesser in 2020, indicating precipitation pattern variation over GMC. The areas
373 covered in dense vegetation are also being consumed by the expanding built-up area. The
374 present study is the report of newly produced data BC and BrC for the fragile region of the
375 Himalayas and its relation with meteorological conditions. It has been observed that the
376 temperature over Gangtok is increasing as well. The peak concentration of BC/BrC has been
377 found during October 2021, March 2021, and 2022. The diurnal distribution of BC/BrC
378 suggests the two peaks in a day, first at 8-10 AM and second at 9-11 PM. The meteorological
379 conditions for the same have been observed to be favorable to diurnal variation of BC/BrC
380 concentration. The monthly variation of the BC/BrC delineated the peak concentration of BC,
381 BC_{bb}, and BC_{ff}, during March 2022. However, BrC and BB% have maximum concentration
382 during April 2021. BB% and BrC as well as BB and carbon dioxide have a strong significant
383 positive correlation coefficient, which is evidence that biomass burning is a substantial factor
384 in the rise in carbon dioxide levels. In addition to this, there is a strong, positive correlation
385 between CO₂ and BC/BC_{ff}, indicating that burning fossil fuels is also one of the causes of
386 rising CO₂ levels. The net thermal radiation, net solar radiation, and BC, BrC relationship
387 suggested that BC and BrC have positive radiative forcing. Furthermore, the monsoon months
388 show the lowest concentrations of BC, BC_{bb}, BC_{ff}, BrC, and BB%, demonstrating the
389 convective rain (i.e., rain out scavenging) ability to remove a majority of contaminants. Both
390 the BC and BrC reveal evidence of positive radiative feedback.

391 **Data Availability**

392 Data is provided in the ‘supplementary section’ and for further detail knowledge about it can
393 be available from the corresponding author on the adequate request.

394 Data link for the data access:

395 [https://docs.google.com/spreadsheets/d/1N4F_ft68syY6n0UIfA6nzI5o-](https://docs.google.com/spreadsheets/d/1N4F_ft68syY6n0UIfA6nzI5o-8LUWjyFfk5NpfquRyg/edit?usp=sharing)
396 [8LUWjyFfk5NpfquRyg/edit?usp=sharing](https://docs.google.com/spreadsheets/d/1N4F_ft68syY6n0UIfA6nzI5o-8LUWjyFfk5NpfquRyg/edit?usp=sharing)

397 **Conflict of Interest**

398 None conflict of interest.

399 **Authors Contribution**

400 Dr. Pramod Kumar: conceptualization, drafting, writing, figures, and editing

401 Ms. Khushboo Sharma: sampling, data analysis, and figures.

402 Ms. Ankita Malu: data analysis, figures, and editing

403 Mr. Rajeev Rajak: editing

404 Ms. Aparna Gupta: editing

405 Mr. Bidyutjyoti Baruah: editing

406 Mr. Jayant Sharma: sampling

407 Dr. Shailesh Yadav: editing, and mentoring

408 Dr. Thupstan Angchuk: editing, and mentoring

409 Dr. Rakesh Kumar Ranjan: conceptualization, data interpretation, mentoring, and editing.

410 Dr. Nishchal Wanjari: editing and mentoring.

411 Dr. Anil Kumar Misra: editing and mentoring.

412 **Acknowledgments**

413 Authors acknowledge to the Department of Science and Technology, Government of India,
414 and host department “DST’s Centre of Excellence (CoE), at Department of Geology, Sikkim
415 University, DST/CCP/CoE/186/2019 (G),” for the generation of BC/BrC data. We also
416 acknowledge to free data sources used in the study as ERA5, and USGS earth explorer.
417 Authors appreciate freely available software such as R-studio, QGIS, CDO, and GrADS used
418 for the analysis and visualization. We also acknowledge Anirud Rai, Kuldeep Dutta, Abhinav
419 Tiwari, Richard Rai, and the anonymous persons who so ever have helped and supported the
420 Black Carbon data collection.

421 **References**

422 Adeeyo, R.O., Edokpayi, J.N., Volenzo, T.E., Odiyo, J.O. and Piketh, S.J., (2022).
423 Determinants of solid fuel use and emission risks among households: insights from Limpopo,
424 South Africa. *Toxics*, 10(2), p.67. <https://doi.org/10.3390/toxics10020067>

425 Aithal, B. H., & MC, C. (2019). Assessing land surface temperature and land use change
426 through spatio-temporal analysis: a case study of select major cities of India. *Arabian Journal*
427 *of Geosciences*, 12(11), 1-16. <https://doi.org/10.1007/s12517-019-4547-1>

428 Ayompe, L.M., Davis, S.J. and Egoh, B.N., (2021). Trends and drivers of African fossil fuel
429 CO₂ emissions 1990–2017. *Environmental Research Letters*, 15(12), p.124039. DOI
430 10.1088/1748-9326/abc64f

431 Benesty, J., Chen, J., Huang, Y., and Cohen, I. (2009). Pearson correlation coefficient. In *Noise*
432 *reduction in speech processing* (pp. 1-4). Springer, Berlin, Heidelberg.
433 https://doi.org/10.1007/978-3-642-00296-0_5

434 Bharali, C., Nair, V. S., Chutia, L., & Babu, S. S. (2019). Modeling of the effects of wintertime
435 aerosols on boundary layer properties over the Indo Gangetic Plain. *Journal of Geophysical*
436 *Research: Atmospheres*, 124(7), 4141-4157. <https://doi.org/10.1029/2018JD029758>

437 Bhat, M. A., Romshoo, S. A., & Beig, G. (2022). Characteristics, source apportionment and
438 long-range transport of black carbon at a high-altitude urban centre in the Kashmir valley,
439 North-western Himalaya. *Environmental Pollution*, 305, 119295.
440 <https://doi.org/10.1016/j.envpol.2022.119295>

441 Bisht, D.S., Dumka, U.C., Kaskaoutis, D.G., Pipal, A.S., Srivastava, A.K., Soni, V.K., Attri,
442 S.D., Sateesh, M. and Tiwari, S., (2015). Carbonaceous aerosols and pollutants over Delhi
443 urban environment: temporal evolution, source apportionment and radiative forcing. *Science*
444 *of the Total Environment*, 521, 431-445. <https://doi.org/10.1016/j.scitotenv.2015.03.083>

445 Biswas, J. and Bhattacharya, S., (2023). Future changes in monsoon extreme climate indices
446 over the Sikkim Himalayas and West Bengal. *Dynamics of Atmospheres and Oceans*, 101,
447 p.101346. <https://doi.org/10.1016/j.dynatmoce.2022.101346>

448 Bond, T. C., Streets, D. G., Yarber, K. F., Nelson, S. M., Woo, J. H., & Klimont, Z. (2004). A
449 technology-based global inventory of black and organic carbon emissions from combustion.
450 *Journal of Geophysical Research: Atmospheres*, 109(D14).
451 <https://doi.org/10.1029/2003JD003697>

452 Brooks, J., Liu, D., Allan, J.D., Williams, P.I., Haywood, J., Highwood, E.J., Kompalli, S.K.,
453 Babu, S.S., Satheesh, S.K., Turner, A.G. and Coe, H., (2019). Black carbon physical and
454 optical properties across northern India during pre-monsoon and monsoon seasons.
455 *Atmospheric Chemistry and Physics*, 19(20), pp.13079-13096. [https://doi.org/10.5194/acp-19-](https://doi.org/10.5194/acp-19-13079-2019)
456 [13079-2019](https://doi.org/10.5194/acp-19-13079-2019)

457 Chiodo, G., Polvani, L.M., Marsh, D.R., Stenke, A., Ball, W., Rozanov, E., Muthers, S. and
458 Tsigaridis, K., (2018). The response of the ozone layer to quadrupled CO₂ concentrations.
459 *Journal of Climate*, 31(10), pp.3893-3907. doi: 10.1175/jcli-d-19-0086.1

460 Davis, W.J., (2017). The relationship between atmospheric carbon dioxide concentration and
461 global temperature for the last 425 million years. *Climate*, 5(4), p.76.
462 <https://doi.org/10.3390/cli5040076>

463 Evangelista, H., Maldonado, J., Godoi, R.H.M., Pereira, E.B., Koch, D., Tanizaki-Fonseca, K.,
464 Van Grieken, R., Sampaio, M., Setzer, A., Alencar, A. and Gonçalves, S.C. (2007). Sources
465 and transport of urban and biomass burning aerosol black carbon at the South–West Atlantic
466 Coast. *Journal of Atmospheric Chemistry*, 56(3), 225-238. [https://doi.org/10.1007/s10874-](https://doi.org/10.1007/s10874-006-9052-8)
467 [006-9052-8](https://doi.org/10.1007/s10874-006-9052-8)

468 Ge, B., Xu, D., Wild, O., Yao, X., Wang, J., Chen, X., Tan, Q., Pan, X. and Wang, Z., (2021).
469 Inter-annual variations of wet deposition in Beijing from 2014–2017: implications of below-
470 cloud scavenging of inorganic aerosols. *Atmospheric Chemistry and Physics*, 21(12), pp.9441-
471 9454. <https://doi.org/10.5194/acp-21-9441-2021>

472 Gupta, P., Singh, S. P., Jangid, A., & Kumar, R. (2017). Characterization of black carbon in
473 the ambient air of Agra, India: Seasonal variation and meteorological influence. *Advances in*
474 *Atmospheric Sciences*, 34(9), 1082-1094. <https://doi.org/10.1007/s00376-017-6234-z>

475 Hansen, A. D. A., & Schnell, R. C. (2005). *The aethalometer*. Magee Scientific Company,
476 Berkeley, California, USA, 7.

477 Hansen, J., Lacis, A., Rind, D., Russell, G., Stone, P., Fung, I., Ruedy, R. and Lerner, J. (1984).
478 *Climate sensitivity: Analysis of feedback mechanisms*. feedback, 1, 1-3.

479 Helin, A., Virkkula, A., Backman, J., Pirjola, L., Sippula, O., Aakko-Saksa, P., Väätäinen, S.,
480 Mylläri, F., Järvinen, A., Bloss, M. and Aurela, M. (2021). Variation of absorption Ångström
481 exponent in aerosols from different emission sources. *Journal of Geophysical Research:*
482 *Atmospheres*, 126(10), 2020JD034094. <https://doi.org/10.1029/2020JD034094>

483 Hersbach, H., Bell, B., Berrisford, P., Hirahara, S., Horányi, A., Muñoz-Sabater, J., Nicolas,
484 J., Peubey, C., Radu, R., Schepers, D. and Simmons, A. (2020). The ERA5 global reanalysis.
485 *Quarterly Journal of the Royal Meteorological Society*, 146(730), 1999-2049.
486 <https://doi.org/10.1002/qj.3803>

487 Huang, Y., Xia, Y. and Tan, X., (2017). On the pattern of CO₂ radiative forcing and poleward
488 energy transport. *Journal of Geophysical Research: Atmospheres*, 122(20), pp.10-578.
489 <https://doi.org/10.1002/2017JD027221>

490 Igarashi, S., Sasaki, H. & Honda, M. (1988). Influence of pressure gradient upon boundary
491 layer stability and transition. *Acta Mechanica* 73, 187–198.
492 <https://doi.org/10.1007/BF01177038>

493 Johnson, R.H. and Hamilton, P.J., (1988). The relationship of surface pressure features to the
494 precipitation and airflow structure of an intense midlatitude squall line. *Monthly Weather*
495 *Review*, 116(7), pp.1444-1473. [https://doi.org/10.1175/1520-](https://doi.org/10.1175/1520-0493(1988)116<1444:TROSPF>2.0.CO;2)
496 [0493\(1988\)116<1444:TROSPF>2.0.CO;2](https://doi.org/10.1175/1520-0493(1988)116<1444:TROSPF>2.0.CO;2)

497 Johnson, M.A., Garland, C.R., Jagoe, K., Edwards, R., Ndemere, J., Weyant, C., Patel, A.,
498 Kithinji, J., Wasirwa, E., Nguyen, T. and Khoi, D.D., (2019). In-home emissions performance
499 of cookstoves in Asia and Africa. *Atmosphere*, 10(5), p.290.
500 <https://doi.org/10.3390/atmos10050290>

501 Jung, K.H., Goodwin, K.E., Perzanowski, M.S., Chillrud, S.N., Perera, F.P., Miller, R.L. and
502 Lovinsky-Desir, S., (2021). Personal exposure to black carbon at school and levels of
503 Fractional Exhaled nitric Oxide in New York city. *Environmental Health Perspectives*, 129(9),
504 p.097005. <https://doi.org/10.1289/EHP8985>

505 Jung, C.H., Lee, H.M., Park, D., Yoon, Y.J., Choi, Y., Um, J., Lee, S.S., Lee, J.Y. and Kim,
506 Y.P., (2023). Parameterization of below-cloud scavenging for polydisperse fine mode aerosols
507 as a function of rain intensity. *Journal of Environmental Sciences*, 132, pp.43-55.
508 <https://doi.org/10.1016/j.jes.2022.07.031>

509 Karra, K., Kontgis, C., Statman-Weil, Z., Mazzariello, J. C., Mathis, M., & Brumby, S. P.
510 (2021). Global land use/land cover with Sentinel 2 and deep learning. In 2021 IEEE
511 international geoscience and remote sensing symposium IGARSS (pp. 4704-4707). IEEE.
512 <https://doi.org/10.1109/IGARSS47720.2021.9553499>

513 Kedia, S., Ramachandran, S., Holben, B. N., & Tripathi, S. N. (2014). Quantification of aerosol
514 type, and sources of aerosols over the Indo-Gangetic Plain. *Atmospheric Environment*, 98,
515 607-619. <https://doi.org/10.1016/j.atmosenv.2014.09.022>

516 Kirchstetter, T. W., Novakov, T., & Hobbs, P. V. (2004). Evidence that the spectral
517 dependence of light absorption by aerosols is affected by organic carbon. *Journal of*
518 *Geophysical Research: Atmospheres*, 109(D21). <https://doi.org/10.1029/2004JD004999>

519 Kiran, V. R., Talukdar, S., Ratnam, M. V., & Jayaraman, A. (2018). Long-term observations
520 of black carbon aerosol over a rural location in southern peninsular India: Role of dynamics
521 and meteorology. *Atmospheric Environment*, 189, 264-274.
522 <https://doi.org/10.1016/j.atmosenv.2018.06.020>

523 Kakkar, A., Rai, P.K., Mishra, V.N. and Singh, P., (2022). Decadal trend analysis of rainfall
524 patterns of past 115 years & its impact on Sikkim, India. *Remote Sensing Applications: Society*
525 *and Environment*, 26, p.100738. <https://doi.org/10.1016/j.rsase.2022.100738>

526 Klimont, Z., Kupiainen, K., Heyes, C., Purohit, P., Cofala, J., Rafaj, P., Borcken-Kleefeld, J.
527 and Schöpp, W. (2017). Global anthropogenic emissions of particulate matter including black
528 carbon. *Atmospheric Chemistry and Physics*, 17(14), 8681-8723. [https://doi.org/10.5194/acp-](https://doi.org/10.5194/acp-17-8681-2017)
529 [17-8681-2017](https://doi.org/10.5194/acp-17-8681-2017)

530 Kumar, M., Parmar, K. S., Kumar, D. B., Mhawish, A., Broday, D. M., Mall, R. K., &
531 Banerjee, T. (2018a). Long-term aerosol climatology over Indo-Gangetic Plain: Trend,
532 prediction and potential source fields. *Atmospheric environment*, 180, 37-50.
533 <https://doi.org/10.1016/j.atmosenv.2018.02.027>

534 Kumar, M., Raju, M. P., Singh, R. S., & Banerjee, T. (2017). Impact of drought and normal
535 monsoon scenarios on aerosol induced radiative forcing and atmospheric heating in Varanasi
536 over middle Indo-Gangetic Plain. *Journal of Aerosol Science*, 113, 95-107.
537 <https://doi.org/10.1016/j.jaerosci.2017.07.016>

538 Kumar, P., Patton, A. P., Durant, J. L., & Frey, H. C. (2018b). A review of factors impacting
539 exposure to PM_{2.5}, ultrafine particles and black carbon in Asian transport microenvironments.
540 *Atmospheric environment*, 187, 301-316. <https://doi.org/10.1016/j.atmosenv.2018.05.046>

541 Kumar, R. R., Soni, V. K., & Jain, M. K. (2020a). Evaluation of spatial and temporal
542 heterogeneity of black carbon aerosol mass concentration over India using three year
543 measurements from IMD BC observation network. *Science of the Total Environment*, 723,
544 138060. <https://doi.org/10.1016/j.scitotenv.2020.138060>

545 Kumar, P., Sharma, M.C., Saini, R. and Singh, G.K., (2020b). Climatic variability at Gangtok
546 and Tadong weather observatories in Sikkim, India, during 1961–2017. Scientific reports,
547 10(1), p.15177. <https://doi.org/10.1038/s41598-020-71163-y>

548 Kumar, P. and Sharma, M.C., 2023. Frontal changes in medium-sized glaciers in Sikkim, India
549 during 1988–2018: Insights for glacier-climate synthesis over the Himalaya. Iscience, 26(10).
550 DOI: 10.1016/j.isci.2023.107789

551 Kurokawa, J. and Ohara, T., (2020). Long-term historical trends in air pollutant emissions in
552 Asia: Regional Emission inventory in ASia (REAS) version 3. Atmospheric Chemistry and
553 Physics, 20(21), pp.12761-12793. <https://doi.org/10.5194/acp-20-12761-2020>

554 Laskin, A., Laskin, J., & Nizkorodov, S. A. (2015). Chemistry of atmospheric brown carbon.
555 Chemical reviews, 115(10), 4335-4382. <https://doi.org/10.1021/cr5006167>

556 Lee, T., Fisher, M., & Schwarz, W. (1995). Investigation of the effects of a compliant surface
557 on boundary-layer stability. Journal of Fluid Mechanics, 288, 37-58.
558 doi:10.1017/S0022112095001054

559 Li, S., Zhang, H., Wang, Z., Chen, Y. (2023a). Advances in the Research on Brown Carbon
560 Aerosols: Its Concentrations, Radiative Forcing, and Effects on Climate. Aerosol Air Qual.
561 Res. 23, 220336. <https://doi.org/10.4209/aaqr.220336>

562 Lin, J., Guo, Y., Li, J., Shao, M. and Yao, P., (2023b). Spatial and temporal characteristics of
563 carbon emission and sequestration of terrestrial ecosystems and their driving factors in
564 mainland China—a case study of 352 prefectural administrative districts. Frontiers in Ecology
565 and Evolution, 11, p.1169427. <https://doi.org/10.3389/fevo.2023.1169427>

566 Liu, D., He, C., Schwarz, J.P. and Wang, X., (2020). Lifecycle of light-absorbing carbonaceous
567 aerosols in the atmosphere. NPJ Climate and Atmospheric Science, 3(1), p.40.
568 <https://doi.org/10.1038/s41612-020-00145-8>

569 Liu, C., Huang, J., Tao, X., Deng, L., Fang, X., Liu, Y., Luo, L., Zhang, Z., Xiao, H.W. and
570 Xiao, H.Y., (2021). An observational study of the boundary-layer entrainment and impact of
571 aerosol radiative effect under aerosol-polluted conditions. Atmospheric Research, 250,
572 p.105348. <https://doi.org/10.1016/j.atmosres.2020.105348>

573 Mahmood, R., Pielke Sr, R.A., Hubbard, K.G., Niyogi, D., Bonan, G., Lawrence, P., McNider,
574 R., McAlpine, C., Etter, A., Gameda, S. and Qian, B. (2010). Impacts of land use/land cover
575 change on climate and future research priorities. Bulletin of the American Meteorological
576 Society, 91(1), 37-46. <https://doi.org/10.1175/2009BAMS2769.1>

577 Massabò, D., Caponi, L., Bernardoni, V., Bove, M.C., Brotto, P., Calzolari, G., Cassola, F.,
578 Chiari, M., Fedi, M.E., Fermo, P. and Giannoni, M. (2015). Multi-wavelength optical
579 determination of black and brown carbon in atmospheric aerosols. Atmospheric Environment,
580 108,1-12. <https://doi.org/10.1016/j.atmosenv.2015.02.058>

581 Moosmüller, H., Chakrabarty, R. K., Ehlers, K. M., & Arnott, W. P. (2011a). Absorption
582 Ångström coefficient, brown carbon, and aerosols: basic concepts, bulk matter, and spherical
583 particles. Atmospheric Chemistry and Physics, 11(3), 1217-1225.
584 <https://doi.org/10.1021/acs.estlett.8b00118>

585 Moteki, N., (2023). Climate-relevant properties of black carbon aerosols revealed by in situ
586 measurements: a review. *Progress in Earth and Planetary Science*, 10(1), pp.1-16.
587 <https://doi.org/10.1186/s40645-023-00544-4>

588 Ohata, S., Moteki, N., Mori, T., Koike, M. and Kondo, Y., (2016). A key process controlling
589 the wet removal of aerosols: new observational evidence. *Scientific reports*, 6(1), p.34113.
590 <https://doi.org/10.1038/srep34113>

591 Osborne, S. R., Johnson, B. T., Haywood, J. M., Baran, A. J., Harrison, M. A. J., & McConnell,
592 C. L. (2008). Physical and optical properties of mineral dust aerosol during the Dust and
593 Biomass-burning Experiment. *Journal of Geophysical Research: Atmospheres*, 113(D23).
594 <https://doi.org/10.1029/2007JD009551>

595 Park, RJ, Kim, MJ, Jeong, JI, Youn, D., & Kim, S. (2010). A contribution of brown carbon
596 aerosol to the aerosol light absorption and its radiative forcing in East Asia. *Atmospheric*
597 *Environment*, 44 (11), 1414-1421. <https://doi.org/10.1016/j.atmosenv.2010.01.042>

598 Pearson, K. (1909). Determination of the coefficient of correlation. *Science*, 30(757), 23-25.
599 [DOI:10.1126/science.30.757.23](https://doi.org/10.1126/science.30.757.23)

600 Pierrehumbert, R. T. (2014). Short-lived climate pollution. *Annual Review of Earth and*
601 *Planetary Sciences*, 42, 341-379. [DOI: 10.1146/annurev-earth-060313-054843](https://doi.org/10.1146/annurev-earth-060313-054843)

602 Prabhu, V., Soni, A., Madhwal, S., Gupta, A., Sundriyal, S., Shridhar, V., Sreekanth, V. and
603 Mahapatra, P.S., (2020). Black carbon and biomass burning associated high pollution episodes
604 observed at Doon valley in the foothills of the Himalayas. *Atmospheric Research*, 243,
605 p.105001. <https://doi.org/10.1016/j.atmosres.2020.105001>

606 Rahman, H., Karuppaiyan, R., Senapati, P.C., Ngachan, S.V. and Kumar, A., (2012). An
607 analysis of past three decade weather phenomenon in the mid-hills of Sikkim and strategies
608 for mitigating possible impact of climate change on agriculture. *Climate change in Sikkim:*
609 *Patterns, impacts and initiatives*, pp.1-18. [http://sikkimforest.gov.in/climate-change-in-](http://sikkimforest.gov.in/climate-change-in-sikkim/2-chapter-An%20analysis%20of%20past%20three%20decade%20weather.pdf)
610 [sikkim/2-chapter-An%20analysis%20of%20past%20three%20decade%20weather.pdf](http://sikkimforest.gov.in/climate-change-in-sikkim/2-chapter-An%20analysis%20of%20past%20three%20decade%20weather.pdf)

611 Ramachandran, S., & Rupakheti, M. (2022). Trends in the types and absorption characteristics
612 of ambient aerosols over the Indo-Gangetic Plain and North China Plain in last two decades.
613 *Science of The Total Environment*, 831, 154867.
614 <https://doi.org/10.1016/j.scitotenv.2022.154867>

615 Ramachandran, S., Rupakheti, M., & Lawrence, M. G. (2020). Black carbon dominates the
616 aerosol absorption over the Indo-Gangetic Plain and the Himalayan foothills. *Environment*
617 *international*, 142, 105814. <https://doi.org/10.1016/j.envint.2020.105814>

618 Ramanathan, V., & Carmichael, G. (2008). Global and regional climate changes due to black
619 carbon. *Nature geoscience*, 1(4), 221-227. <https://doi.org/10.1038/ngeo156>

620 Rana, A., Rawat, P. and Sarkar, S., (2023). Sources, transport pathways and radiative effects
621 of BC aerosol during 2018–2020 at a receptor site in the eastern Indo-Gangetic Plain.
622 *Atmospheric Environment*, p.119900. <https://doi.org/10.1016/j.atmosenv.2023.119900>

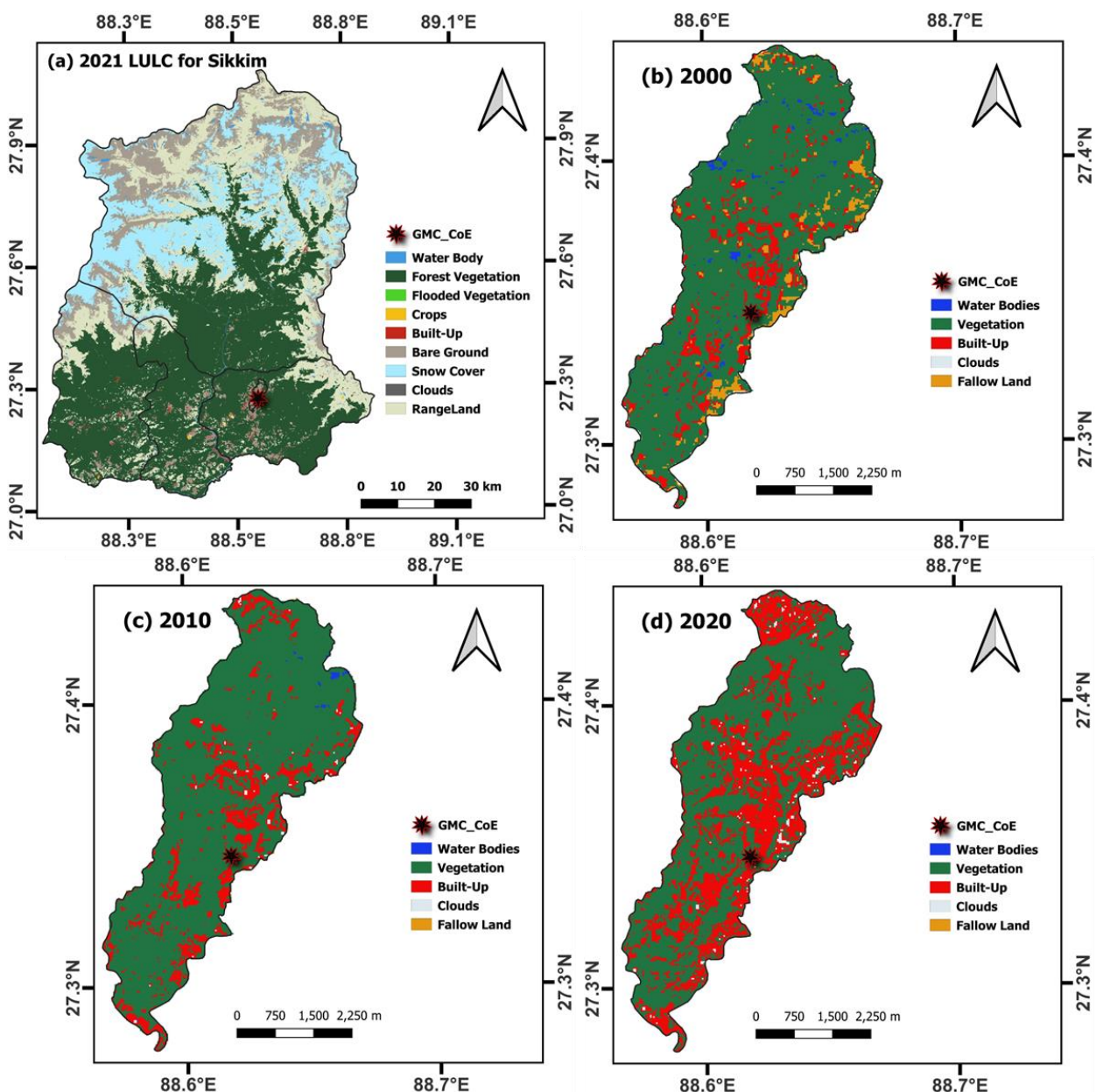
623 Rathod, T. D., & Sahu, S. K. (2022). Measurements of optical properties of black and brown
624 carbon using multi-wavelength absorption technique at Mumbai, India. *Journal of Earth*
625 *System Science*, 131(1), 32. <https://doi.org/10.1007/s12040-021-01774-0>

- 626 Rathod, T., Sahu, S. K., Tiwari, M., Yousaf, A., Bhangare, R. C., & Pandit, G. G. (2017). Light
627 absorbing properties of brown carbon generated from pyrolytic combustion of household
628 biofuels. *Aerosol and Air Quality Research*, 17(1), 108-116.
629 <https://doi.org/10.4209/aaqr.2015.11.0639>
- 630 Reddy, M. S., & Venkataraman, C. (2002a). Inventory of aerosol and sulphur dioxide
631 emissions from India: I—Fossil fuel combustion. *Atmospheric Environment*, 36(4), 677-697.
632 [https://doi.org/10.1016/S1352-2310\(01\)00463-0](https://doi.org/10.1016/S1352-2310(01)00463-0)
- 633 Reddy, M. S., & Venkataraman, C. (2002b). Inventory of aerosol and sulphur dioxide
634 emissions from India. Part II—biomass combustion. *Atmospheric Environment*, 36(4), 699-
635 712. [https://doi.org/10.1016/S1352-2310\(01\)00464-2](https://doi.org/10.1016/S1352-2310(01)00464-2)
- 636 Runa, F., Islam, M., Jeba, F., & Salam, A. (2022). Light absorption properties of brown carbon
637 from biomass burning emissions. *Environmental Science and Pollution Research*, 29(14),
638 21012-21022. <https://doi.org/10.1007/s11356-021-17220-z>
- 639 Sankar, T.K., Ambade, B., Mahato, D.K., Kumar, A. and Jangde, R., (2023). Anthropogenic
640 fine aerosol and black carbon distribution over urban environment. *Journal of Umm Al-Qura*
641 *University for Applied Sciences*, pp.1-10. <https://doi.org/10.1007/s43994-023-00055-4>
- 642 Sarkar, A., (2018). A generalized relationship between atmospheric pressure and precipitation
643 associated with a passing weather system. *MAUSAM*, 69(1), pp.133-140. DOI:
644 10.54302/mausam.v69i1.242
- 645 Sharma, K., Ranjan, R.K., Lohar, S., Sharma, J., Rajak, R., Gupta, A., Prakash, A. and Pandey,
646 A.K. (2022). Black Carbon Concentration during Spring Season at High Altitude Urban Center
647 in Eastern Himalayan Region of India. *Asian Journal of Atmospheric Environment (AJAE)*,
648 16(1). <https://doi.org/10.5572/ajae.2021.149>
- 649 Shindell, D., Kuylensstierna, J.C., Vignati, E., van Dingenen, R., Amann, M., Klimont, Z.,
650 Anenberg, S.C., Muller, N., Janssens-Maenhout, G., Raes, F. and Schwartz, J. (2012).
651 Simultaneously mitigating near-term climate change and improving human health and food
652 security. *Science*, 335(6065), 183-189. DOI: [10.1126/science.1210026](https://doi.org/10.1126/science.1210026)
- 653 Shaddick, G., Thomas, M.L., Mudu, P., Ruggeri, G. and Gumy, S., (2020). Half the world's
654 population are exposed to increasing air pollution. *NPJ Climate and Atmospheric Science*,
655 3(1), p.23. <https://doi.org/10.1038/s41612-020-0124-2>
- 656 Shukla, K. K., Sarangi, C., Attada, R., & Kumar, P. (2022). Characteristic dissimilarities
657 during high aerosol loading days between western and eastern Indo-Gangetic Plain.
658 *Atmospheric Environment*, 269, 118837. <https://doi.org/10.1016/j.atmosenv.2021.118837>
- 659 Sloss, L. (2012). Black carbon emissions in India. CCC/209. IEA Clean Coal Centre, London,
660 38.
- 661 Stevens, B., & Feingold, G. (2009). Untangling aerosol effects on clouds and precipitation in
662 a buffered system. *Nature*, 461(7264), 607-613. <https://doi.org/10.1038/nature08281>
- 663 Stjern, C.W., Forster, P.M., Jia, H., Jouan, C., Kasoar, M.R., Myhre, G., Olivié, D., Quaas, J.,
664 Samset, B.H., Sand, M. and Takemura, T., (2023). The Time Scales of Climate Responses to
665 Carbon Dioxide and Aerosols. *Journal of Climate*, 36(11), pp.3537-3551.
666 <https://doi.org/10.1175/JCLI-D-22-0513.1>

- 667 Sun, Y., Hao, Q., Cui, C., Shan, Y., Zhao, W., Wang, D., Zhang, Z. and Guan, D., (2022).
668 Emission accounting and drivers in East African countries. *Applied Energy*, 312, p.118805.
669 <https://doi.org/10.1016/j.apenergy.2022.118805>
- 670 Takemura, T., & Suzuki, K. (2019). Weak global warming mitigation by reducing black carbon
671 emissions. *Scientific reports*, 9(1), 1-6. <https://doi.org/10.1038/s41598-019-41181-6>
- 672 Venkataraman, C., Habib, G., Kadamba, D., Shrivastava, M., Leon, J.F., Crouzille, B.,
673 Boucher, O. and Streets, D.G. (2006). Emissions from open biomass burning in India:
674 Integrating the inventory approach with high-resolution Moderate Resolution Imaging
675 Spectroradiometer (MODIS) active-fire and land cover data. *Global biogeochemical cycles*,
676 20(2). <https://doi.org/10.1029/2005GB002547>
- 677 Watham, T., Padalia, H., Srinet, R., Nandy, S., Verma, P. A., & Chauhan, P. (2021). Seasonal
678 dynamics and impact factors of atmospheric CO₂ concentration over subtropical forest
679 canopies: observation from eddy covariance tower and OCO-2 satellite in Northwest
680 Himalaya, India. *Environmental Monitoring and Assessment*, 193(2), 1-15.
681 <https://doi.org/10.1007/s10661-021-08896-4>
- 682 Wang, Q., Liu, H., Ye, J., Tian, J., Zhang, T., Zhang, Y., Liu, S. and Cao, J., (2020). Estimating
683 Absorption Ångström Exponent of Black Carbon Aerosol by Coupling Multiwavelength
684 Absorption with Chemical Composition. *Environmental Science & Technology Letters*, 8(2),
685 pp.121-127. <https://doi.org/10.1021/acs.estlett.0c00829>
- 686 Wang, L., Jin, W., Sun, J., Zhi, G., Li, Z., Zhang, Y., Guo, S., He, J. and Zhao, C., (2021).
687 Seasonal features of brown carbon in northern China: Implications for BrC emission control.
688 *Atmospheric Research*, 257, p.105610. <https://doi.org/10.1016/j.atmosres.2021.105610>
- 689 Wu, Y., Wang, Y., Zhou, Y., Liu, X., Tang, Y., Wang, Y., Zhang, R. and Li, Z., (2022). The
690 wet scavenging of air pollutants through artificial precipitation enhancement: A case study in
691 the Yangtze River Delta. *Frontiers in Environmental Science*, 10, p.1027902.
692 <https://doi.org/10.3389/fenvs.2022.1027902>
- 693 Xiao-lei, C. H. U., L. U. Zhong, W. E. I. Dan, and L. E. I. Guo-ping., (2022). Effects of land
694 use/cover change on temporal and spatial variability of precipitation and temperature in the
695 Songnen Plain of China. *Journal of Integrative Agriculture* 21, no. 1: 235. doi: 10.1016/S2095-
696 3119(20)63495-5
- 697 Yasunari, T., Bonasoni, P., Laj, P., Fujita, K., Vuillermoz, E., Marinoni, A., Cristofanelli, P.,
698 Duchi, R., Tartari, G. and Lau, K.M. (2010). Estimated impact of black carbon deposition
699 during pre-monsoon season from Nepal Climate Observatory–Pyramid data and snow albedo
700 changes over Himalayan glaciers. *Atmospheric Chemistry and Physics*, 10(14), 6603-6615.
701 <https://doi.org/10.5194/acp-10-6603-2010>
- 702 Yoo, J.M., Lee, Y.R., Kim, D., Jeong, M.J., Stockwell, W.R., Kundu, P.K., Oh, S.M., Shin,
703 D.B. and Lee, S.J., (2014). New indices for wet scavenging of air pollutants (O₃, CO, NO₂,
704 SO₂, and PM₁₀) by summertime rain. *Atmospheric Environment*, 82, pp.226-237.
705 <https://doi.org/10.1016/j.atmosenv.2013.10.022>
- 706 Yue, S., Zhu, J., Chen, S., Xie, Q., Li, W., Li, L., Ren, H., Su, S., Li, P., Ma, H. and Fan, Y.
707 (2022). Brown carbon from biomass burning imposes strong circum-Arctic warming. *One*
708 *Earth*, 5(3), 293-304. <https://doi.org/10.1016/j.oneear.2022.02.006>

- 709 Zhang, R., Jing, J., Tao, J., Hsu, S.-C., Wang, G., Cao, J., Lee, C. S. L., Zhu, L., Chen, Z.,
710 Zhao, Y., and Shen, Z. (2013). Chemical characterization and source apportionment of PM2.5
711 in Beijing: seasonal perspective, *Atmos. Chem. Phys.*, 13, 7053–7074,
712 <https://doi.org/10.5194/acp-13-7053-2013>
- 713 Zhang, A., Wang, Y., Zhang, Y., Weber, R.J., Song, Y., Ke, Z. and Zou, Y., (2020). Modeling
714 the global radiative effect of brown carbon: a potentially larger heating source in the tropical
715 free troposphere than black carbon. *Atmospheric Chemistry and Physics*, 20(4), pp.1901-1920.
716 <https://doi.org/10.5194/acp-20-1901-2020>
- 717 Zhu, C.S., Qu, Y., Huang, H., Chen, J., Dai, W.T., Huang, R.J. and Cao, J.J., (2021). Black
718 carbon and secondary brown carbon, the dominant light absorption and direct radiative forcing
719 contributors of the atmospheric aerosols over the Tibetan Plateau. *Geophysical research letters*,
720 48(11), p.e2021GL092524. <https://doi.org/10.1029/2021GL092524>

List of Figures



722

723 Figure 1. The study location and land use land cover for 2000, 2010, 2020, and 2021 for
724 December over Gangtok and Sikkim region using Landsat-5, Landsat-8, and Sentinel-2 data
725 sets.

726

727

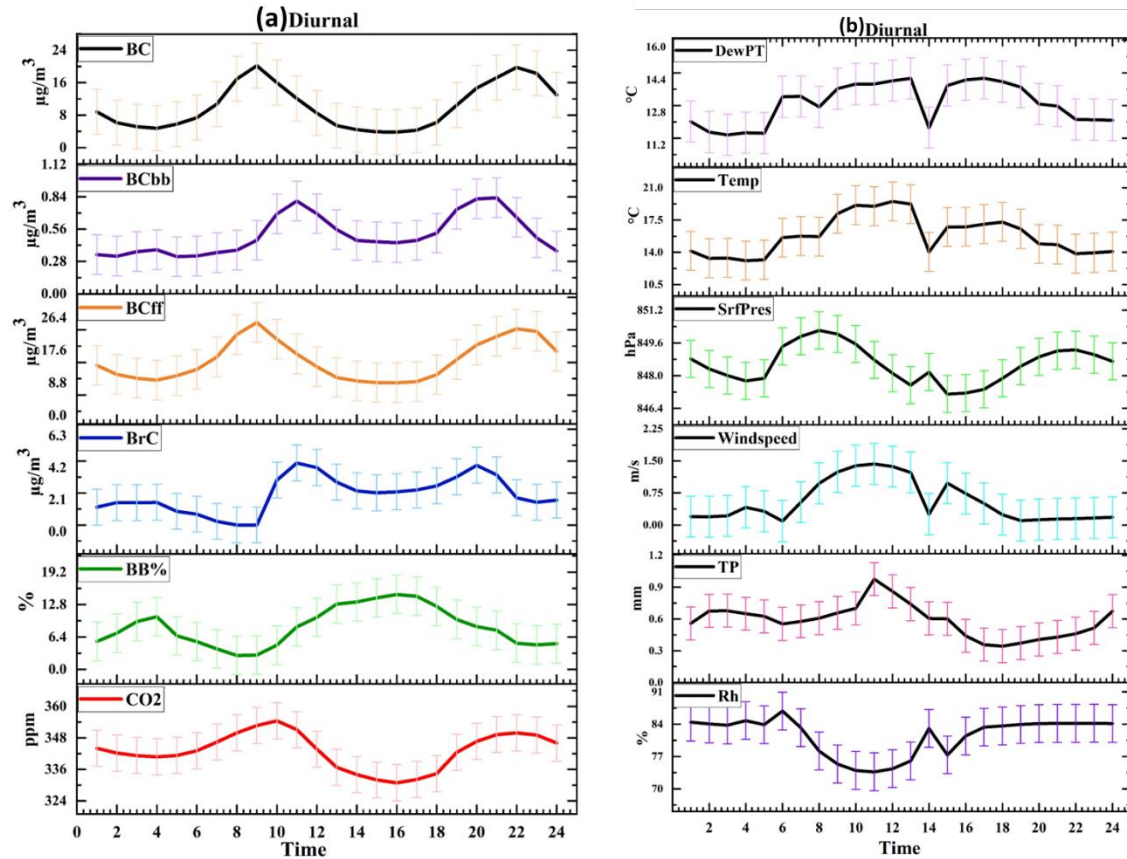
728

729

730

731

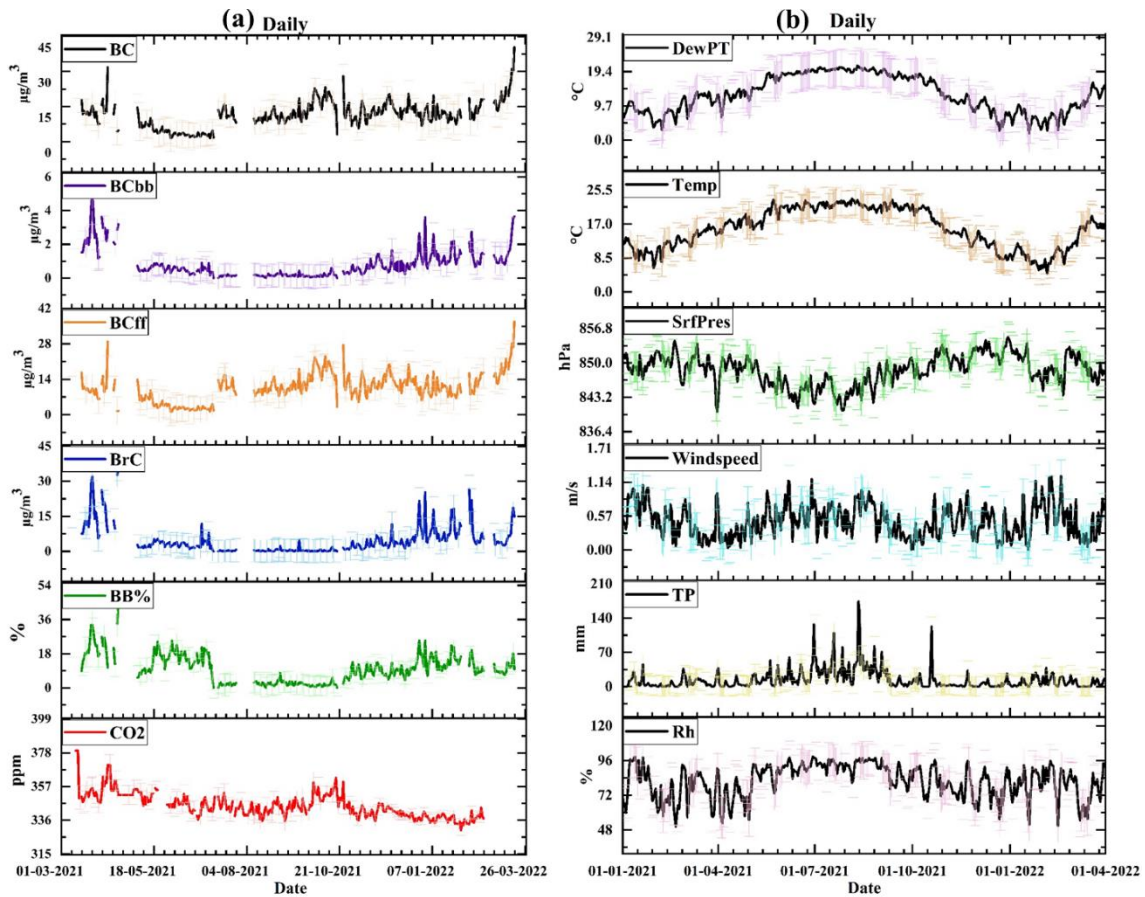
732



734

735 Figure 2. (a) The hourly observation of Black Carbon, Black Carbon through biomass burning,
 736 Black Carbon through fossil fuel, Brown Carbon, Biomass Burning percentage and Carbon
 737 Dioxide (BC, BC_{bb}, BC_{ff}, BrC, BB%, and CO₂, respectively) (The corresponding unit for BC,
 738 BC_{bb}, BC_{ff}, BrC: $\mu\text{g}/\text{m}^3$; BB%: % and CO₂: ppm) for 16th March 2021 to 10th March 2022 over
 739 study location (lat:27.32; lon:88.61). The light colour shading refers to $\pm\sigma$ standard deviation
 740 for each variable. (b) Same as Figure 2a, but for meteorological parameters such as dewpoint
 741 temperature (DewPT), temperature (Temp), surface pressure (SrfPres), windspeed, total
 742 precipitation (TP), and relative humidity (Rh) from 16th March 2021 to 10th March 2022.

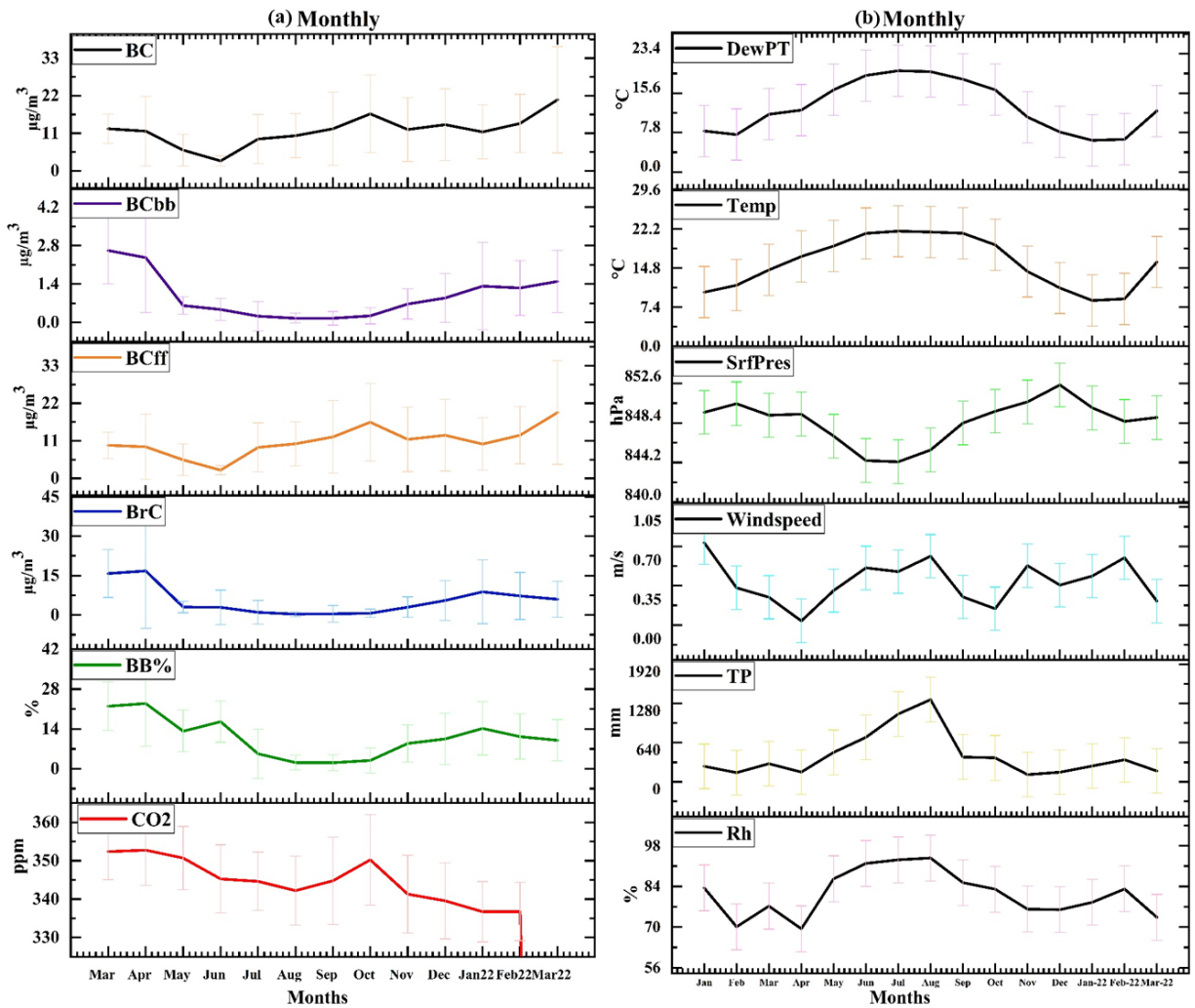
743



744

745 Figure 3. (a) The daily mean of Black Carbon, Black Carbon through biomass burning, Black
 746 Carbon through fossil fuel, Brown Carbon, Biomass Burning percentage and Carbon Dioxide
 747 (BC, BC_{bb}, BC_{ff}, BrC, BB%, and CO₂, respectively) (The corresponding unit for BC, BC_{bb},
 748 BC_{ff}, BrC: $\mu\text{g}/\text{m}^3$; BB%: % and CO₂: ppm) for 16th March 2021 to 10th March 2022 over study
 749 location (lat:27.32; lon:88.61). The light colour shading refers to $\pm\sigma$ standard deviation for
 750 each variable. (b) same as Figure 3a, but for meteorological parameters such as dewpoint
 751 temperature (DewPT), temperature (Temp), surface pressure (SrfPres), Windspeed, total
 752 precipitation (TP), and relative humidity (Rh) from 1st January 2021 to 31st March 2022.

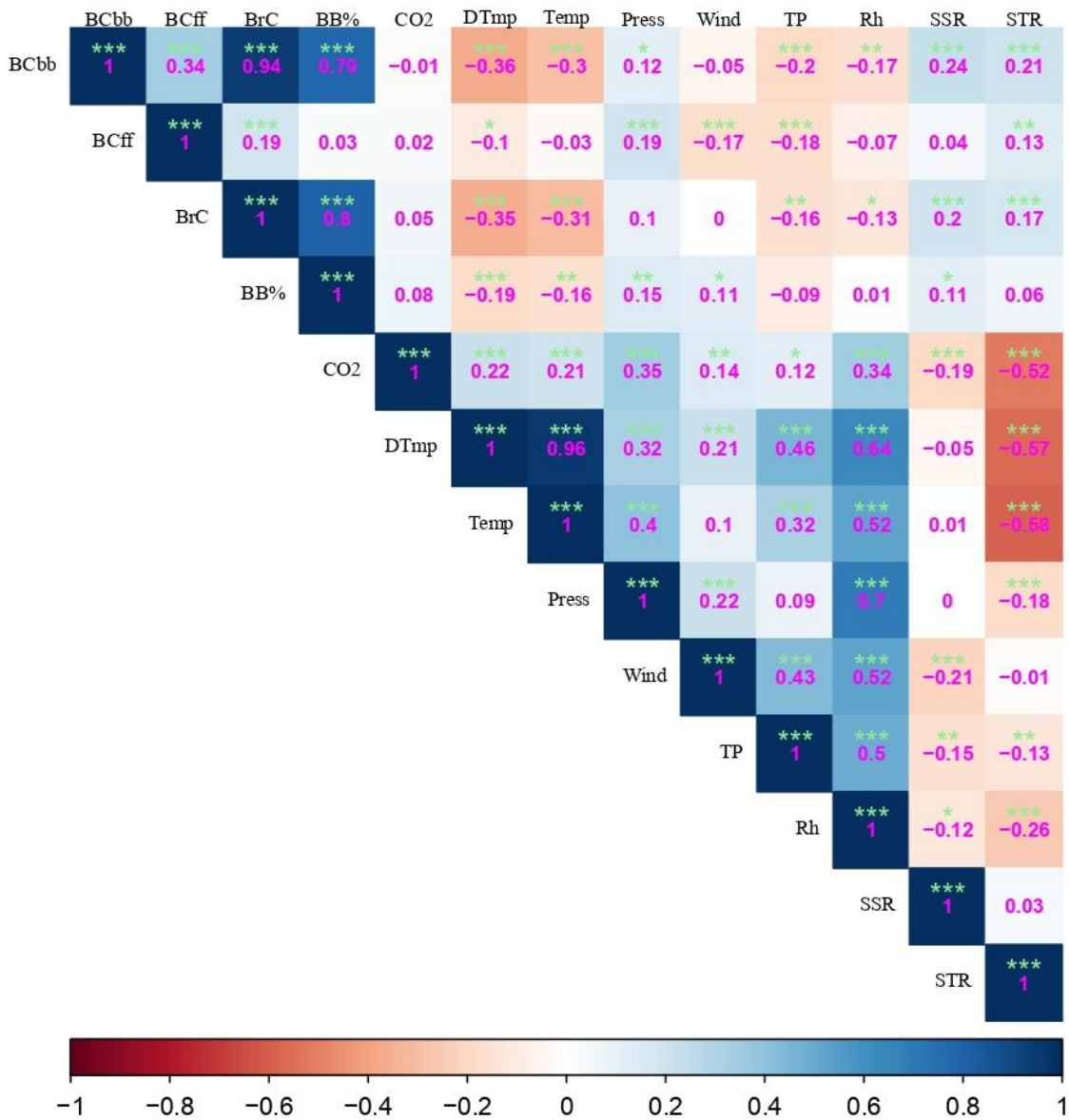
753



754

755 Figure 4. (a) The monthly mean of Black Carbon, Black Carbon through biomass burning,
 756 Black Carbon through fossil fuel, Brown Carbon, Biomass Burning percentage and Carbon
 757 Dioxide (BC, BC_{bb}, BC_{ff}, BrC, BB%, and CO₂, respectively) (The corresponding unit for BC,
 758 BC_{bb}, BC_{ff}, BrC: $\mu\text{g}/\text{m}^3$; BB%: % and CO₂: ppm) for 16th March 2021 to 10th March 2022 over
 759 study location (lat:27.32; lon:88.61). The error bar shows $\pm\sigma$ standard deviation for each
 760 variable. (b) Same as Figure 4a, but for meteorological parameters such as dewpoint
 761 temperature (DewPT), temperature (Temp), surface pressure (SrfPres), windspeed, total
 762 precipitation (TP), and relative humidity (Rh) during January 2021 to March 2022.

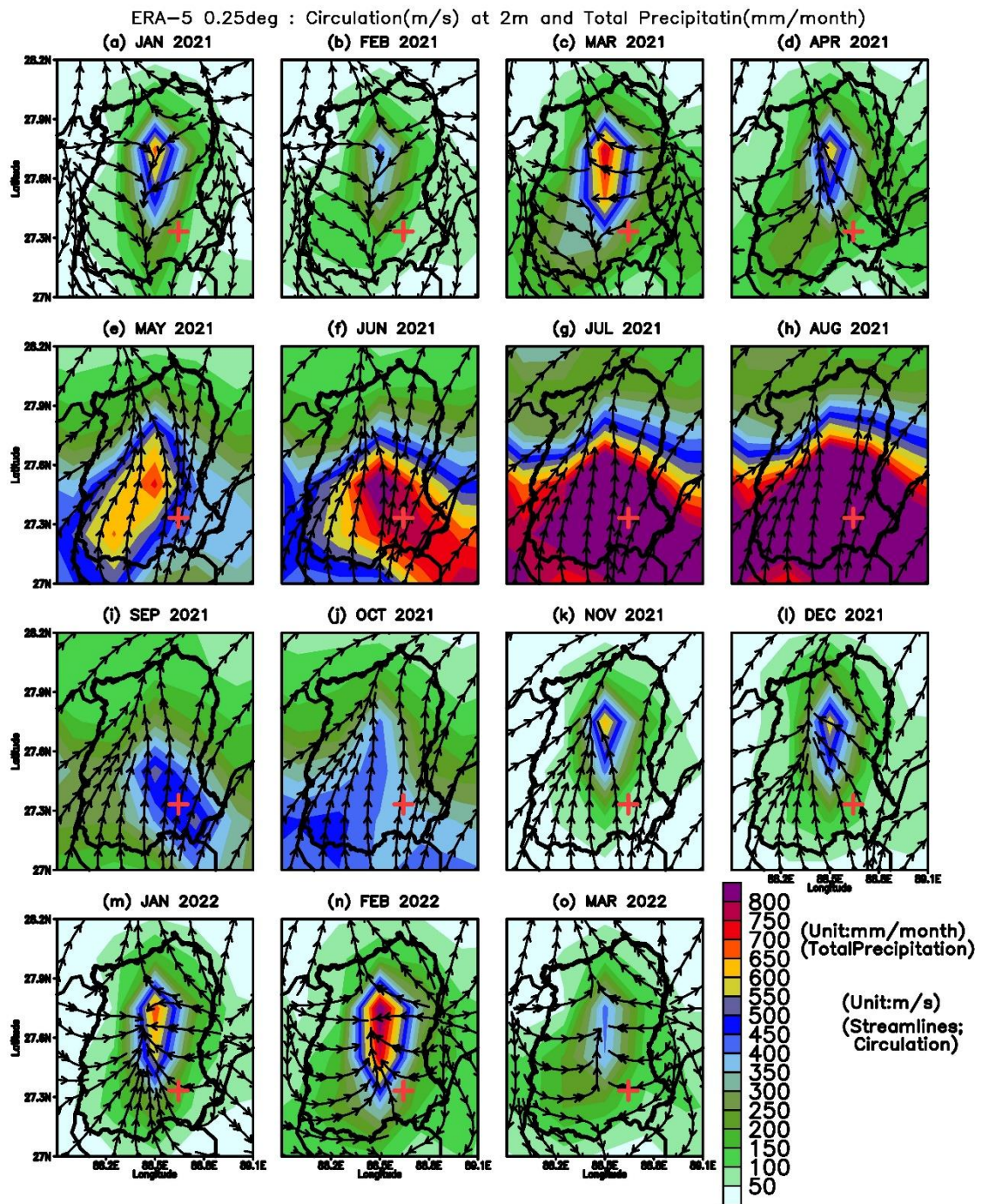
763



764

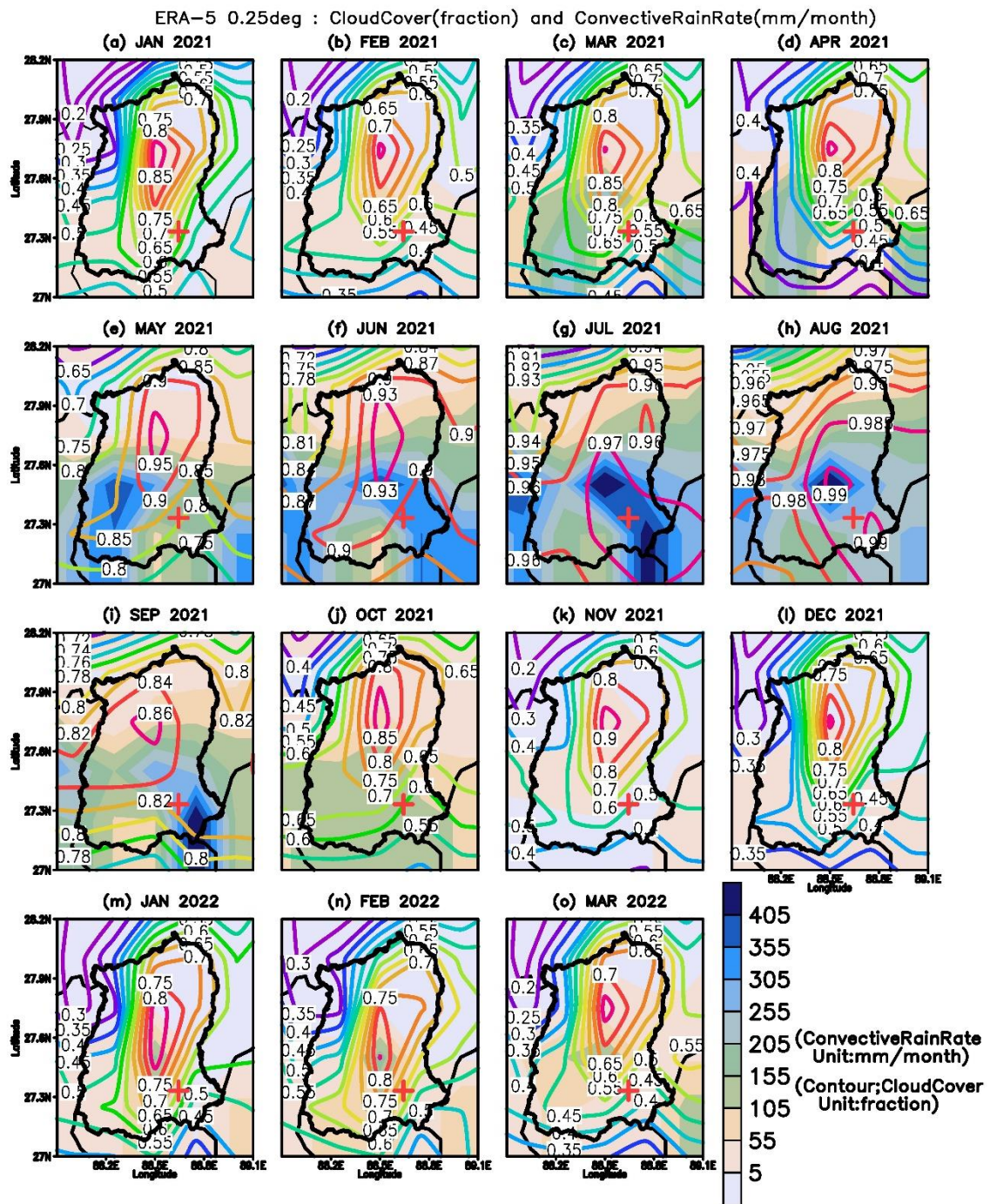
765 Figure 5. Correlation among BC, BC_{bb}, BC_{ff}, BrC, BB%, CO₂ and, dewpoint temperature
 766 (DTmp), temperature (Temp), surface pressure (Press), Wind, total precipitation (TP), Relative
 767 humidity (Rh), net solar radiation (SSR), and net thermal radiation (STR). The (***) shows
 768 99% significance, (**) shows 95% significance, (*) 90% significance, and () shows no
 769 significance. The correlation coefficient values (-0.3 to -0.49) or (0.3 to 0.49) are considered
 770 ‘a good correlation’, and values ≤ (-0.5) or ≥ (0.5) are considered “a strong correlation”.

771



772 Figure 6. Monthly total precipitation (cumulative) and wind circulation pattern during January
 773 2021 to March 2022. The Shading shows precipitation patterns, and the streamline shows wind
 774 circulation. The (+) mark is a representation of the sampling location.

775



776 Figure 7. Monthly convective rain and total cloud cover during January 2021 to March 2022.
 777 The shading shows a convective rain pattern, and the contour shows a total cloud cover
 778 fraction. The (+) mark is a representation of the sampling location.

779

780

List of Tables

781 Table 1. The details of datasets used for the present study.

782

Variables	Data sets	Years (Span)	Resolution		Source	Reference
			Temporal	Horizontal		
Black and Brown Carbon	Observation and analysis, data generated using Aethalometer AE33	March 2021-March 2022	Weekly	Point Location (Gangtok)	Original data generated	Present Study
Total precipitation	ERA5 (ECMWF)	2021 to 2022	Hourly	0.25° * 0.25°	ECMWF https://cds.climate.copernicus.eu/cdsapp#!/dataset/reanalysis-era5-single-levels?tab=form	Hersbach et al., 2020
Relative humidity						
Temperature (2 meter)						
Wind (surface wind)						
Surface pressure						
Dewpoint temperature						
Net solar, and thermal radiation downward						
LULC	LandSat-5, LandSat-8 and earth explorer USGS	December 2000, December 2010, December 2020	2000, 2010, 2020	30m, 30m	earth explorer USGS. https://earthexplorer.usgs.gov/	earth explorer USGS.
LULC	Sentinel-2 Esri Inc.	December 2021	2021	10 m	Esri Inc. https://www.arcgis.com/home/item.html?id=d3da5dd386d140cf93fc9ecbf8da5e31	Karra et al., 2021

783